In situ Study of the Crystallization from Amorphous to Cubic Zirconium Oxide: Rietveld and Reverse Monte Carlo Analyses

Feng Zhang,[†] Peter J. Chupas,[‡,§] Siu Lun Alan Lui,[†,||] Jonathan C. Hanson,[⊥] Wolfgang A. Caliebe,[#,○] Peter L. Lee,[◇] and Siu-Wai Chan*[,†]

Department of Applied Physics & Applied Mathematics and MRSEC center, Columbia University, New York, New York 10027, Department of Chemistry, State University of New York at Stony Brook, Stony Brook, New York 11794, Department of Chemistry and National Synchrotron Light Source, Brookhaven National Laboratory, Upton, New York 48824, and Advanced Photon Source, Argonne National Laboratory, Argonne, Illinois 60439

Received July 25, 2006. Revised Manuscript Received April 10, 2007

The amorphous-to-cubic (a−c) crystallization of nanoZrO_2 in a reducing environment was studied by synchrotron X-ray diffraction. Rietveld analysis was performed to study the changes in crystallite size and lattice parameter as the cubic phase emerged. The pair distribution function (PDF) was obtained from the Fourier transformation of the normalized XRD patterns. A reverse Monte Carlo (RMC) simulation was applied to provide details of the local structure during the crystallization process as well as to calculate partial PDFs of Zr−Zr and Zr−O during the crystallization. The number of Zr's next-nearest neighbors of Zr remains 12, whereas the number of O's as nearest neighbors of Zr increases from 6.7 to 7.3 as the material evolves from an amorphous into a cubic structure, suggesting the persistence of a high concentration of oxygen vacancies. These simulated atomic structures show that the local structure of the amorphous phase bears resemblance to the short-range arrangement of cubic ZrO_2, consistent with the results of X-ray absorption near edge spectroscopy (XANES) at Zr L_{II} and L_{III}. The amorphous-to-crystalline phase transformation is affected by the environment. Under an oxidizing condition, the amorphous phase crystallizes directly to tetragonal and subsequently to monoclinic zirconia.

1. Introduction

Zirconium oxide is an important engineering ceramic for various applications, as electrolytes of solid oxide fuel cells, high-temperature structural ceramics, and thermal barrier materials.[1−3] Recently, zirconia has been considered as an important candidate for the replacement of SiO_2 as the gate oxide in microelectronic devices because of its high permittivity, large band gap, and good thermal and chemical stability on silicon.[4]

Zirconia has three polymorphs, as shown in Table 1. The transitions between different phases of zirconium oxide have been widely investigated.[5−6] In general, the monoclinic form is the stable phase at room temperature. At elevated temperatures (>1170 °C), the tetragonal phase becomes stable, followed by the cubic phase at even higher temperatures (>2370 °C). By adding appropriate dopants, i.e., CaO and Y_2O_3, cubic and tetragonal phases can be stabilized at room temperature. It is also demonstrated that tetragonal phase can be obtained at room temperature by decreasing the particle size.[7] The stabilization of high-temperature phases at room temperature was explained to be enhanced by oxygen vacancies, stress, surface energy, and fine crystalline size.[7−9] In particular, in ceria−zirconia nanoparticles, the cubic fluorite phase was stabilized to a higher zirconia concentration through a particle-size effect[10] and a reducing environment.[11]

Extended X-ray absorption fine structure spectroscopy (EXAFS) has been widely used to study the local structures of zirconia polymorphs.[12−16] All polymorphs of ZrO_2 can

* Corresponding author. E-mail: sc174@columbia.edu.
[†] Columbia University.
[‡] State University of New York at Stony Brook.
[§] Now at Materials Science Division, Argonne National Laboratory, Argonne, Illinois 60439.
[||] Visiting student from Chinese University of Hong Kong, Hong Kong SAR, P. R. China.
[⊥] Department of Chemistry, Brookhaven National Laboratory.
[#] National Synchrotron Light Source, Brookhaven National Laboratory.
[○] Now at Hasylab am Desy, Hamburg, Germany.
[◇] Argonne National Laboratory.

(1) Stevens, R. *An Introduction to Zirconia and Zirconia Ceramics*, 2nd ed.; Magnesium Elektron Ltd.: Twikenham, UK, 1986.
(2) Steele, B. C. H.; Heinzel, A. *Nature* **2001**, *414* (6861), 345.
(3) Whittemore, O. J., Jr.; Ault, N. N. *J. Am. Ceram. Soc.* **1956**, *39* (12), 442.
(4) Copel, M.; Gribelyuk, M.; Gusev, E. *Appl. Phys. Lett.* **2000**, *76* (4), 436.
(5) Heuer, A. H.; Hobbs, L. W. *Science and Technology of Zirconia*; The American Ceramic Society: Westerville, OH, 1981.
(6) Claussen, N.; Ruhle, M. *Science and Technology of Zirconia II*; The American Ceramic Society: Westerville, OH, 1984.
(7) Mitsuhashi, T.; Ichihara, M.; Tatsuke, U. *J. Am. Ceram. Soc.* **1974**, *57* (2), 97.
(8) Fabris, S.; Paxton, A. T.; Finnis, M. W. *Acta Mater.* **2002**, *50*, 5171.
(9) Garvie, R. C.; Goss, M. F. *J. Mater. Sci.* 1986, *21*, 1253.
(10) Zhang, F.; Chen, C.-H.; Hanson, J. C.; Robinson, R. D.; Herman, I. P.; Chan, S.-W. *J. Am. Ceram. Soc.* **2006**, *89*, 1028−1036.
(11) Zhang, F.; Raitano J. M.; Chen, C.-H.; Hanson, J. C.; Wolfgang, C.; Khalid, S.; Chan, S.-W. *J. Appl. Phys.* **2006**, *99*, 0843131−0843138.
(12) Li, P.; Chen, I.-W.; Penner-Hahn, J. E. *Phys. Rev. B* **1993**, *48* (14), 10063.
(13) Li, P.; Chen, I.-W.; Penner-Hahn, J. E. *Phys. Rev. B* **1993**, *48* (14), 10074.
(14) Li, P.; Chen, I.-W.; Penner-Hahn, J. E. *Phys. Rev. B* **1993**, *48* (14), 10082.
(15) Winterer, M. *J. Appl. Phys.* **2000**, *88* (10), 5635.

10.1021/cm061739w CCC: $37.00
Published on Web 06/02/2007

Table 1. Polymorphs of ZrO_2 from the Joint Committee on Powder Diffraction File (JCPDF) Database

JCPDF no.	phase	space group	*a* (Å)	*b* (Å)	*c* (Å)	β (deg)	details
37-1484	monoclinic	*P*21/*a*	5.3129	5.2125	5.1471	99.218	
42-1164	tetragonal	*P*42/*nmc*	3.64		5.27	90	
49-1642	cubic	$Fm\bar{3}m$	5.1280			90	oxygen deficient ZrO_x, $x = 1.688-1.740$

be treated as local distortions of the cubic fluorite structure.[12] It is found that the Zr−O bondings are similar among the cubic, orthorhombic, and monoclinic phases, with a coordination number close to 7 for Zr^{4+}. On the other hand, tetragonal phase has a Zr−O coordination number of 8 for Zr^{4+}, resembling a layered structure close to the fluorite structure.[12] Table 1 lists the corresponding lattice parameters of the cubic, tetragonal, and monoclinic crystal structures of zirconia. Few studies have been conducted on amorphous zirconia and even fewer have given details of the local structure during the crystallization process of the amorphous to cubic ZrO_2.[15]

The study of crystallization in situ requires fast collection of data at high temperatures. Recently, Chupas et al. demonstrated the feasibility of using a high-energy synchrotron X-ray source to record high-quality diffraction patterns in short intervals to a large scattering factor, *Q*, with an area detector.[17−18] This instrumental improvement makes the in situ study of the phase transitions possible. Because of the availability of large *Q* values with the synchrotron X-ray source, advanced analyses, such as Rietveld and pair distribution function (PDF) analyses, can be applied to determine the long-range as well as local structures of the different phases.

Rietveld analysis of X-ray diffraction (XRD) is now widely applied to determine the long-range structure of crystalline materials.[19] Atomic positions, site occupancies, lattice parameters, crystallite size, strain, and the thermal factor can be obtained by refining the whole XRD profile through Rietveld analysis.

2. Experimental Section

Materials. Amorphous zirconium oxide was prepared by mixing 0.5 M hexamethylenetetramine (HMT, $C_6N_4H_{12}$, Lancaster, 99+%) with 0.04 M $ZrOCl_2 \cdot 8H_2O$ (Alfa, 99.9%) at room temperature for 24 h. After the sample was centrifuged out as precipitate, it was washed with distilled water and dried in an oven at around 50 °C. The standard samples of Y_2O_3-doped ZrO_2 (Alfa, 99%, 10−15% Y_2O_3, excluding Hf) and pure ZrO_2 (Alfa, 99.5%, Hf < 100 ppm) were checked for phase purity with a Scintag X-ray diffractometer and are referred to as the cubic and monoclinic zirconia standards, respectively.

X-ray Diffraction. The X-ray diffraction experiments were performed at the 1-ID beam line at the Advanced Photon Source (APS) located at Argonne National Laboratory, Argonne, IL. High-energy X-rays were delivered to the experimental hutch using a double bent Laue monochromator, which is capable of providing a flux of 1×10^{12} photons/s and operating with X-rays in the energy range of 80−100 keV.[20] A wavelength as small as 0.1241(2) Å was used to provide a maximum scattering vector *Q* of 24.5 $Å^{-1}$. A Mar345 image plate camera was mounted orthogonal to the beam path, with the beam centered on the image plate. Calibration of wavelength and image plate position was performed using a LaB_6 standard and the software Fit-2d.[21] The sample was mounted in a sealed quartz capillary assembled into an apparatus as previously described for high-temperature experiments.[22] The recording time for each pattern or scan is 1 min and 50 s. Therefore, each pattern is a time average of the evolving XRD pattern over a scan time of 110 s. While recording the patterns, we increased the temperature with a constant rate from room temperature to 500 °C in 2 h with an average heating rate of 4 °C/min, kept it at 500 °C for 20 min, and then rapidly cooled it to room temperature, as shown in Figure 1a. Therefore, except during the dwelling at 500 °C, the temperature varied by 7.5 °C per scan during ramping and decreased by as much as 250 °C between two consecutive scans during rapid cool down, such that even when an average temperature is given, the scan number gives a more accurate account.

Additional experiments of high-temperature in situ XRD were also conducted at beamline X7B at National Synchrotron Light Source (NSLS), Brookhaven National Laboratory, Upton, NY. The experimental setup is similar to the setup at beamline 1-ID at APS, but with a larger wavelength of 0.9200 Å as well as a better control of the gaseous environment. In the reducing experiment, the quartz capillary measuring cell was connected to a vacuum system of which the base vacuum was 5×10^{-6} Torr. A mass spectrometer was connected to the vacuum system to monitor the reaction. In the oxidizing experiment, a gas mixture of 5% O_2/95% He was flowing through the measuring cell.

General Structure Analysis Software[23] with EXP Graphic User Interface[24] was used for the whole-profile Rietveld analysis on crystalline zirconium oxide. PDFgetX software[25] was used to subtract the amorphous quartz background from the pattern, normalize the pattern, and obtain the PDF files. The Q_{max} used in the analysis is 24.5 $Å^{-1}$. The normalization of the experimental spectra is critical for obtaining high-quality PDF spectra as well as further analyses. Instrumental details and theoretical considerations were described earlier.[12] Reverse Monte Carlo (RMC) simulation of PDF was performed on both amorphous and crystalline zirconia with Discus software.[26] Proffen has studied the defect structure of 15% CaO-doped ZrO_2 with different sizes of model crystals by RMC refinement. When the model crystal is large (i.e., $20 \times 20 \times$

(16) Villella, P.; Conradson, S. D.; Espinosa-Faller, F. J.; Foltyn, S. R.; Sickafus, K. E.; Valdez, J. A.; Degueldre, C. A. *Phys. Rev. B* **2001**, *64*, 104101.
(17) Chupas, P. J.; Qiu, X.; Hanson, J. C.; Lee, P. L.; Grey, C. P.; Billinge, S. J. L. *J. Appl. Crystallogr.* **2003**, *36*, 1342−1347.
(18) Chupas, P. J.; Grey, C. P.; Hanson, J. C., J.-Kim, Y.; Rodrigues, J.; Qiu, X.; Billinge, S. J. L.; Lee, P. L. In situ Time-Resolved Powder Diffraction Studies in Heterogeneous Catalysis; Coupling the Study of Long-Range and Local Structural Changes. In *Commission for Powder Diffraction Newsletter No. 29*; International Union of Crystallography: Chester, UK, 2003; p 24.
(19) McCusker, L. B.; Von Dreele, R. B.; Cox, D. E.; Louer, D.; Scardi, P. *J. Appl. Crystallogr.* **1999**, *32*, 36.
(20) Shastri, S. D.; Fezzaa, K.; Mashayekhi, A.; Lee, W. K.; Fernandes, P. B.; Lee, P. L. *J. Synchrotron Radiat.* **2002**, *9*, 317.
(21) Hammersley, A. *FIT2D: 2-D detector calibration/correction; File reformatting; 2-D fitting software*, version V10.132; European Synchrotron Radiation Facility: Grenoble, France, 2001.
(22) Chupas, P. J.; Ciraolo, M. F.; Hanson, J. C.; Grey, C. P. *J. Am. Chem. Soc.* **2001**, *123* (8), 1694.
(23) Larson, A. C.; Von Dreele, R. B. *General Structure Analysis System (GSAS)*; Los Alamos National Laboratory Report LAUR 86-748; Los Alamos National Laboratory: Los Alamos, NM, 2000.
(24) Toby, B. H. *J. Appl. Crystallogr.* **2001**, *34*, 210.
(25) Jeong, I.-K.; Thompson, J.; Proffen, Th., Perez, A.; Billinge, S. J. L. *J. Appl. Crystallogr.* **2001**, *34*, 536.
(26) Proffen, Th.; Neder, R. B. *J. Appl. Crystallogr.* **1997**, *30*, 171.

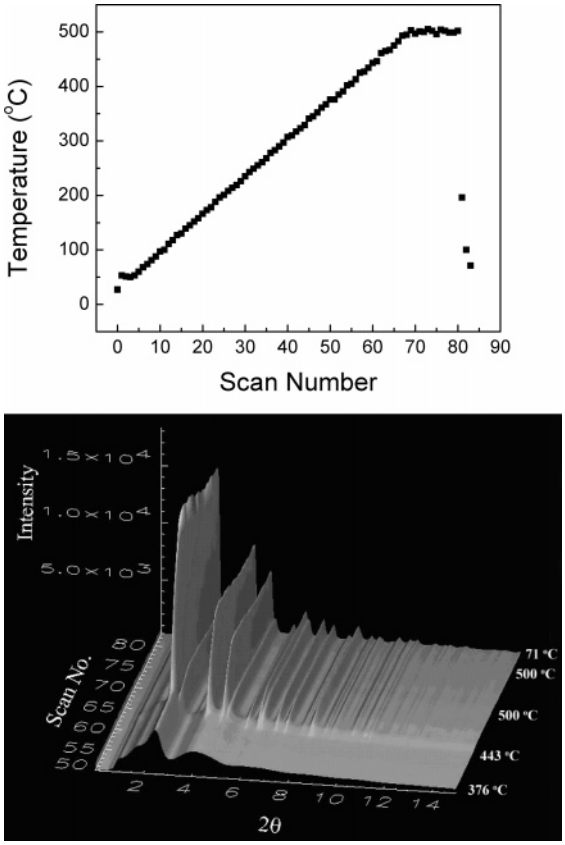

Figure 1. (a) The temperature profile applied while the XRD pattern was recording. Each XRD scan took 1 min and 50 s; 90 scans took a total of 165 min. (b) In situ XRD showing the phase transition from amorphous to cubic ZrO_2 in a reducing environment.

20 unit cells), the simulated diffraction have relatively low noise but the model contains too many degrees of freedom such that the final simulated structure does not necessarily reflect the short-range order inherent in the data. When the model crystal is small (i.e., $5 \times 5 \times 5$ unit cells), although the simulated diffraction has a higher noise level, the number of degrees of freedom becomes manageable and fast convergence is obtained with the final structure often providing important information of the local structure.[27] Therefore, we chose a model crystal of $6 \times 6 \times 6$ unit cells with 2592 ions in this study. For every refinement, the ions were first displaced by a random amount smaller than 0.25 Å. After 40 000 cycles, the displacement was decreased to 0.05 Å, and the refinement was run for more 80 000 cycles. For most simulations, cubic ZrO_2 was used as the starting structure. For several other simulations, fluorite structure with a lattice parameter of 4 Å and tetragonal and monoclinic ZrO_2 were applied as the starting structures. Real space PDF analysis was applied on cubic ZrO_2 with the PDFFit[26] program.

Details of the PDF Method. Pair distribution function (PDF) was first developed to study the local structure of amorphous materials, i.e., liquid and glass.[29] An PDF is obtained by a Fourier transform of the corresponding normalized XRD pattern from reciprocal space to real space.

$$G(r) = 4\pi r(\rho(r) - \rho_o) = \frac{2}{\pi}\int_0^\infty Q(S(Q) - 1)\sin(Qr)\,dQ \quad (1)$$

Here, $G(r)$ is the pair distribution function, $\rho(r)$ is the microscopic pair distribution, ρ_o is the average pair density, Q is the magnitude of the scattering vector where $Q = (4\pi \sin\theta)/\lambda$, $S(Q)$ is the normalized scattering intensity, and r is the ion−ion distance. Usually, PDF analysis is applied to study amorphous materials. In 1990, it was applied to study the local structures and defects in crystalline materials.[30] Such analysis uses both Bragg and diffuse scattering, providing information of both long- and short-range structures.[28,31]

Details of the RMC method. Reverse Monte Carlo (RMC) is another method that serves to determine the structure of amorphous materials. Provided with a starting structure with the same chemical composition as the material being analyzed, the RMC program randomly selects an atom (or an ion) and displaces it by a random distance smaller than a maximum specified beforehand. On the basis of the new structure generated, the software calculates the scattering intensity, compares it with the observed results, and provides a goodness-of-fit number, χ, as shown in eq 2.

$$\chi^2 = \sum_{i=1}^{N} \frac{[I_e(h_i) - I_c(h_i)]^2}{\sigma^2} \quad (2)$$

$$\Delta\chi^2 = \chi_{new}{}^2 - \chi_{old}{}^2 \quad (3)$$

Here, I_e is the experimental intensity, I_c is the calculated intensity, and σ is an independent factor between 0 and 1. If $\Delta\chi^2 < 0$, the movement is accepted by the program. If $\Delta\chi > 0$, the move is accepted with a probability of $\exp(-\Delta\chi^2/2)$. A smaller σ value would result in more bad movements to be rejected. σ is usually in the range of 0.01−0.1. Details of RMC simulation can be found in refs 26, 32, and 33.

XANES. X-ray absorption near edge spectra (XANES) of zirconia polymorphs were collected at the Zr L_{II} and L_{III} edges using fluorescence mode on beamline X-19A at the NSLS. The Si (111) double-crystal monochromator was detuned (monitored by a 50% decrease in the maximum transmitted intensity) to remove the higher-order harmonics. A thin Zr foil was used as the standard to calibrate the energy.

3. Results

3.1. Rietveld Analysis of Cubic ZrO_2. The prepared ZrO_2 remains as an amorphous phase from room temperature to 434 °C (scan no. 59). The formation of the cubic phase occurs quickly between two consecutive scans, nos. 59 and 60. At 443 °C (scan no. 60), ZrO_2 acquires a cubic-fluorite structure with the characteristic XRDs giving a number of well-defined peaks. To provide a better view of the phase transition, we show only XRD patterns after scan no. 50 in Figure 1b. After the initial cubic phase formation, the intensities of these peaks continue to increase with increasing temperature from 443 to 475 °C (i.e., from scan no. 60 to 65), suggesting that the crystallinity of the sample is increasing.

Rietveld analysis has been applied on all the XRD patterns of the cubic phase. Figure 2 shows a typical XRD pattern and the corresponding Rietveld analysis. Only the cubic

(27) Proffen, Th.; Welberry, T. R. *J. Appl. Crystallogr.* **1998**, *31*, 318.
(28) Proffen, Th.; Billinge, S. *J. Appl. Crystallogr.* **1999**, *32*, 572.
(29) Klug, H. P.; Alexander, L. E. *X-ray Diffraction Procedures for Polycrystalline and Amorphous Materials*, 2nd ed.; John Wiley & Sons: New York, 1974.
(30) Egami, T. *J. Phys. Chem. Solids* **1995**, *56* (10), 1407.
(31) Proffen, Th.; Billinge, S. J. L.; Egami, T.; Louca, D. *Kristallogr. Z.* **2003**, *218*, 132.
(32) Mellergard, A.; McGreevy, R. L. *Acta Crystallogr., Sect. A* **1999**, 55, 783.
(33) McGreevy, R. L.; Pusztai, L. *Mol. Simul.* **1988**, *1*, 359.

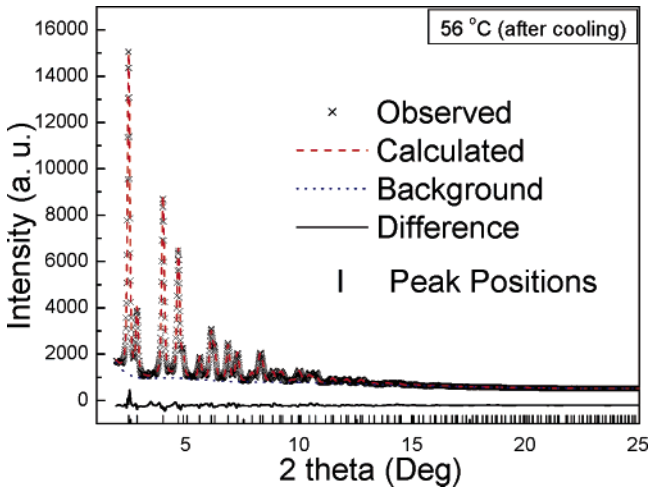

Figure 2. Comparison of observed XRD pattern to the Rietveld analysis of cubic ZrO_2 at 56 °C (after being cooled down).

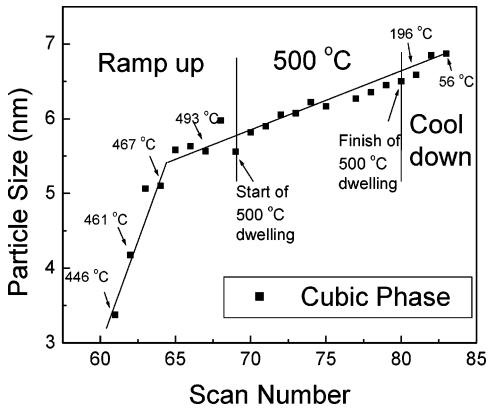

Figure 3. The crystalline size of the cubic phase plotted against scan number with markers indicating the average temperature during the scan for the ramping, soaking at 500 °C, and cooling down regions.

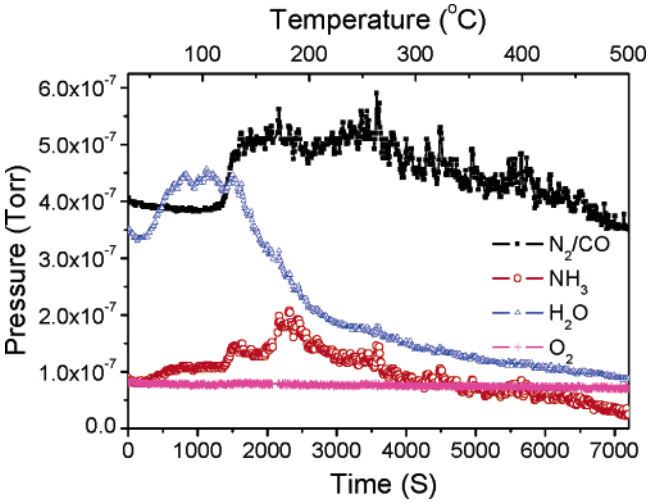

Figure 4. In situ mass spectroscopy study of the gas compositions while amorphous zirconia was annealed.

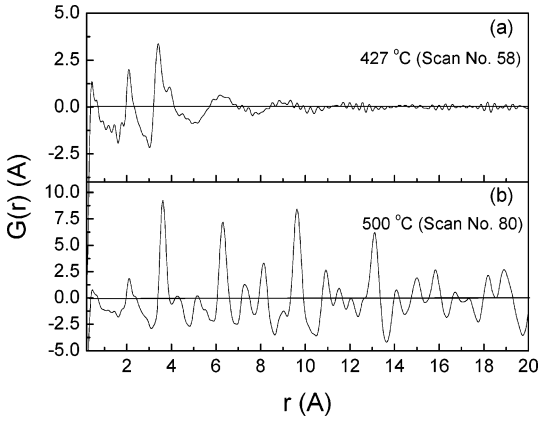

Figure 5. Typical experimental PDF spectra of (a) amorphous and (b) cubic ZrO_2.

phase is identified after the crystallization. The lattice parameter change of cubic ZrO_2 is mainly due to the thermal expansion effect. The crystallite size (Figure 3) shows a rapid growth after crystallization. After the average size reaches 5.5 nm (475 °C, scan no. 65), a slower rate is seen for size increment. As mentioned above, the XRD intensity increases from scan no. 60 to 65. In the early stage, the nuclei grow quickly and consume the surrounding amorphous matrix. When no amorphous zirconia is left, the larger ZrO_2 crystallites grow more slowly by consuming smaller ZrO_2 crystallites, a classic Ostwald ripening case.

3.2. H_2O in Amorphous ZrO_2. When amorphous zirconium oxide is prepared by the wet chemistry method, a considerable amount of chemically absorbed water[34−35] can be found with the extreme composition corresponding to $Zr(OH)_4$. To determine the structure of the amorphous zirconia, it is important to verify the role of water in the amorphous materials studied. In the mass spectroscopy, as shown in Figure 4, the water released from the sample peaks around 100 °C. The water vapor partial pressure then decreases smoothly without any additional peak as the temperature rises. At crystallization temperature, 443 °C, the partial pressure of water vapor is down to the 1×10^{-7} Torr range with no observable change with further heating. Therefore, the water inside the as-prepared amorphous zirconia is physically absorbed, mostly desorbed before reaching 300 °C, and does not affect the crystallization process above 430 °C.

Considerable amounts of CO and NH_3 are released at around 125 °C and beyond (Figure 4). These are the products of the decomposition of HMT. Although the sample was washed after the preparation, some residual HMT was still attached to the surface of the prepared samples. The gaseous products CO and NH_3 from the HMT decomposition resulted in a reducing environment during the annealing.[11]

3.3. Reverse Monte Carlo Analysis. The typical experimental PDF $G(r)$ patterns of amorphous and cubic ZrO_2 are shown in panels a and b of Figure 5. Systematic errors tend to be slowly modulating as a function of Q and therefore manifest themselves as ripples in the low-r region of $G(r)$. These ripples occur at nonphysical distances (i.e., smaller than that of the Zr−O closest contact). Thus, the RMC simulations conducted in this work were carried out over the range 0.8 Å $< r <$ 20 Å. In some cases, small ripples can be seen propagating through $G(r)$, most notably in the PDFs of the amorphous material. These are either from termination effects due to Fourier transform over a finite Q range or from systematic experimental errors. Although PDFs

(34) Yoldas, B. E. *J. Am. Ceram. Soc.* **1982**, *65* (8), 387.
(35) Huang, C.; Tang, Z.; Zhang, Z. *J. Am. Ceram. Soc.* **2001**, *84* (7), 1637.

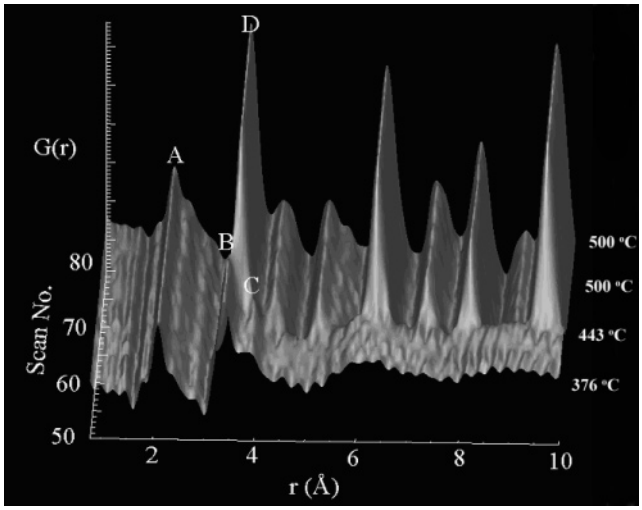

Figure 6. Three-dimensional experimental $G(r)$ showing the evolution of PDF peaks during crystallization.

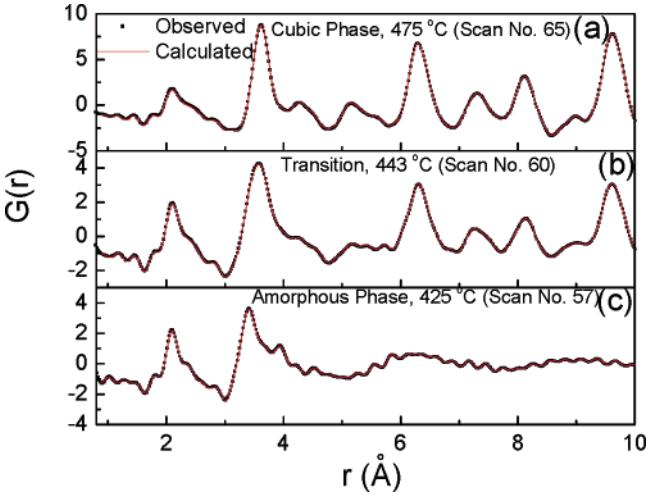

Figure 7. Calculated $G(r)$ values from RMC simulations of (a) cubic, (b) transition, and (c) amorphous zirconia as compared to $G(r)$ values from experiments.

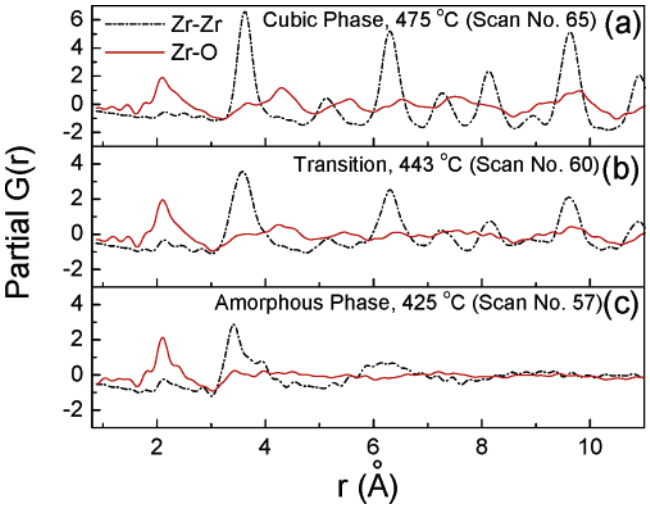

Figure 8. Partial PDFs of Zr−Zr and Zr−O of (a) cubic, (b) transition, and (c) amorphous ZrO_2 calculated from RMC simulations.

of improved quality might be obtained from conventional measurements utilizing solid-state point detectors, the current study makes direct use of the novelty of the time-resolved PDF approach. Results are obtained continuously during the transition from amorphous to crystalline phases and structural changes are determined continuously. Because structural changes are determined continuously, the effect of systematic errors is minimized and valuable information is obtained for the structural transition of amorphous ZrO_2 to crystalline cubic ZrO_2.

Figure 6 shows a plot of all the experimental $G(r)$ values obtained in this study. The PDFs of amorphous ZrO_2 show peaks only at small r values (1−7 Å). As the amorphous material crystallizes, the material starts to show an ordered long-range structure as peaks at large values of r appear. As crystallization proceeds, the cubic phase of ZrO_2 shows well-developed long-range structure. Some short-range structures in the initial amorphous state persist or evolve in the final cubic phase. Peak A at $r = 2.1$ Å, in Figure 6, does not change its position in both phases. In fluorite structure, this distance corresponds to the Zr−O, connecting Zr to its nearest-neighbor oxygens (NN), i.e., 1/4[111]a. Peak B and C of the amorphous phase evolve into peak D during the crystallization. Peak D at $r = 3.6$ Å belongs to the Zr−Zr distance, connecting Zr with its next-nearest-neighbor Zr's (NNN), i.e., 1/2[110]a.

The PDFs obtained from the reverse Monte Carlo (RMC) simulations of the amorphous, crystallization, and crystalline cubic structures are shown in Figure 7. The results from the RMC agree well with the experimental $G(r)$ values. From the RMC simulations and the resultant structures, one can calculate the oxygen and zirconium contributions to the PDFs. Therefore, it is possible to obtain the partial pair distributions for the Zr−Zr and Zr−O correlations. The O−O partial pair distribution is also available from RMC simulations. However, because X-rays are less sensitive to oxygen, the signal from O−O partial pair distribution is small and not as reliable. Partial PDF's of Zr−O and Zr−Zr of different phases from RMC calculation are shown in Figure 8. From the partial PDF's extracted from the RMC simulations, one can obtain the numbers of nearest neighbors (NN) and next-nearest neighbors (NNN) of zirconium in ZrO_2. This information is not available from the total PDF calculated from the experimental data.

$$4\pi r\rho(r) = 4\pi r\rho_o + G(r) \tag{4}$$

$$N_{ab} = \int_a^b (4\pi r\rho_o + G(r))r\,dr \tag{5}$$

where N_{ab} is the pair number of atoms (ions) with an interaction distance ranging from a to b, whereas $G(r)$ is the corresponding partial pair distribution function and $n(r)$ is really $(4\pi r\rho_o+G(r))r$, the pair density. The area under each peak represents the number of Zr−Zr pairs in that distance range. Every peak can be simulated with a Gaussian function, giving the number of Zr neighbors for each spherical shell spanned by the peak. The same approach can be applied to analyze Zr−O pairs. The number of NNN of Zr remains 12 for both the amorphous and cubic phases, as shown in Figure 9, which agrees well with previous results from EXAFS.[12,15] The number of Zr nearest neighbors (Zr−O NN) is monitored as crystallization progresses (Figure 10). Theoretically, this number should be 8 for fluorite structure as in ceria. In $(Zr,Y)O_{1.87}$, the number of cation nearest neighbors is 7.[12]

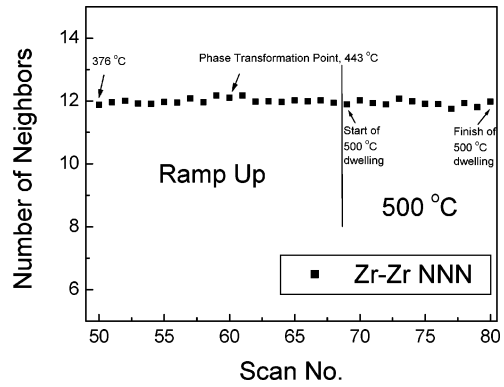

Figure 9. Number of next-nearest neighbors (NNN) for Zr (i.e., Zr−Zr pairs) obtained from RMC calculation.

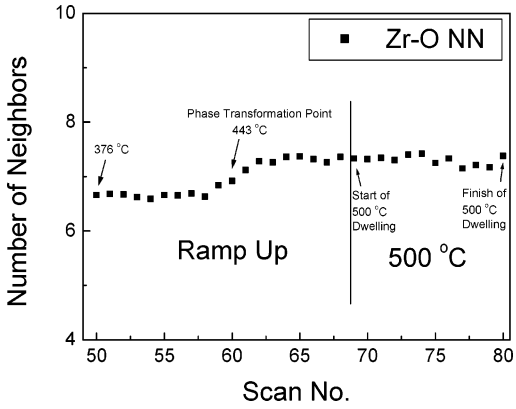

Figure 10. Number of nearest neighbors (NN) of Zr, i.e., Zr−O pairs obtained from RMC calculation.

Here, the number increases from 6.7 in the amorphous phase to 7.3 in the cubic phase.

Three representative structures obtained from RMC simulation are shown in Figure 11 a−c. All the figures are the projections along the (001) direction. For the amorphous phase, although the Zr atoms are random in the long range, they form tetrahedrons locally, as shown in Figure 11d. At the phase transition, besides the zirconium tetrahedron units, some cubic features can be observed, as shown in encircled area of Figure 11b. In the cubic ZrO_2, the features of fluorite structure are fairly clear. (Note here that the starting structure applied is cubic ZrO_2 with lattice parameter be 5.2 Å.) The small oxygen coordination number obtained is mainly due to the displacements of the oxygen ions from their normal sites in fluorite.

Three structures, fluorite structure with lattice parameter of 4 Å, tetragonal (JCPDS file no. 42-1164), and monoclinic ZrO_2 (JCPDS file no. 37-1484), were used as different starting structures in RMC simulation for the amorphous phase. These three structures provided a similar output structure for the amorphous phase. The situation is very different for the RMC simulation of the final cubic phase, where the cubic ZrO_2 starting structure with a lattice parameter of 5.2 Å needs to be used to give satisfactory results. This difference in the requirement of the starting structure to give reasonable results agrees with Winterer's EXAFS RMC simulation results on amorphous zirconia and yttria-stabilized cubic zirconia.[15]

Previous study shows that the existence of oxygen vacancies is important for the stabilization of cubic phase of ZrO_2.[5,6,8,11−14,27] Because the experiments were conducted in a reducing condition, it is necessary to verify the role of oxygen vacancies in the current study. The reason to perform the RMC simulation is to compare the structure of the amorphous phase with the cubic phase. The Rietveld analysis which cannot be applied to the amorphous phase gives structural information for the cubic phase from the PDF spectra. From the Rietveld analysis in Section 3.1, we optimized the lattice parameter, thermal factors, and occupancies of lattice sites. As shown in Figure 12, the real space Rietveld analysis agrees well with experimental reduced $G(r)$ and gives 3% oxygen vacancies from the recorded XRD pattern taken at 500 °C right before cool down. Similar Rietveld analysis of XRD patterns from the subsequent cool down scans gives the same 3% oxygen vacancy concentration. However, if the occupancy of Zr sites is lower from 1 to 0.97, Rietveld analysis can give an oxygen vacancy concentration as high as 16% from the same XRD patterns.

3.4. In situ XRD Study in an Oxidizing Environment. When the amorphous ZrO_2 was annealed in an oxidizing environment ($P_{O_2} = 38$ Torr), the resulting phase from crystallization is different from the cubic phase in a reducing environment ($P_{O_2} = 1 \times 10^{-7}$ Torr) earlier. As shown in Figure 13, at the crystallization, the amorphous phase directly changes into the tetragonal phase. The amorphous to crystalline ZrO_2 phase transition is significantly affected by the annealing environment. Under the reducing atmosphere, amorphous ZrO_2 crystallizes into the cubic phase and remains as the cubic phase at room temperature, no matter how slow the ramping down is. In the oxidizing atmosphere, it crystallizes directly into the tetragonal phase.

After remaining at 530 °C for about 1.5 h, the monoclinic phase nucleates and grows from the tetragonal phase. In the last few scans, both tetragonal and monoclinic phases are present in the pattern. As the zirconia crystalline size is increasing at 530 °C, the phase transformation from tetragonal to monoclinic is promoted by the larger crystallite size.[36]

3.5. XANES at the Zr L_{II} and L_{III} Edge. X-ray absorption near edge spectroscopy (XANES) is associated with the excitation process of core electrons to bound/quasibound states. It provides information of the electron state and local structure. The Zr L_{II} and L_{III} edges in XANES of tetragonal ZrO_2 and cubic (Zr, Ce, Sm)O_{2-x} have been studied before.[37] Two main white lines, which are attributed to the e_g and t_{2g} states, have been found in the cubic phase. These states are associated with different Zr d-orbital levels, z^2, $x^2 - y^2$ for e_g, and xy, yz, and xz for t_{2g}, respectively. The e_g peak is 2.3 eV below the t_{2g} peak. In tetragonal ZrO_2, besides these lines, an additional peak can be observed between them, because of the low crystal symmetry. These results agree well with Orlando's theoretical calculation based on the density functional theory.[38]

(36) Tang, J.; Zhang, F.; Zoogman, P.; Fabbri, J.; Chan, S.-W.; Zhu, Y.; Brus, L. E.; Steigerwald, M. L. *Adv. Mater.* **2005**, *15*, 1595−1602.
(37) Huang, W.; Shuk, P.; Greenblatt, M.; Croft, M.; Chen, F.; Liu, M. *J. Electrochem. Soc.* **2000**, *147* (11), 4196.
(38) Orlando, R.; Pisani, C.; Roetti, C.; Stefanovich, E. *Phys. Rev. B* **1992**, *45* (2), 45592.

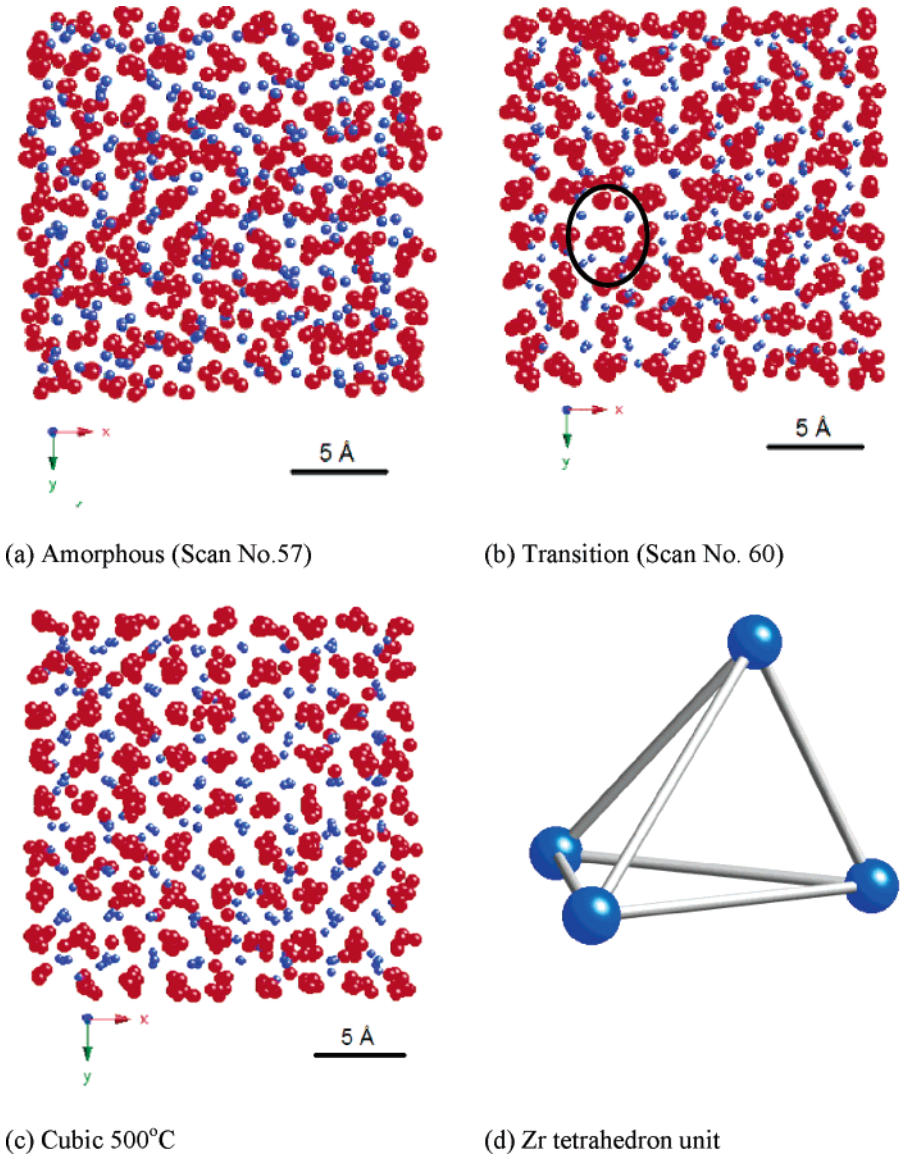

Figure 11. ZrO_2 structures obtained from RMC simulation. Smaller blue spheres are zirconium ions, larger red spheres are oxygen ions. (a) Amorphous (scan no. 57); (b) transition (scan no. 60); (c) cubic 500 °C (scan no. 80); (d) Zr tetrahedron unit.

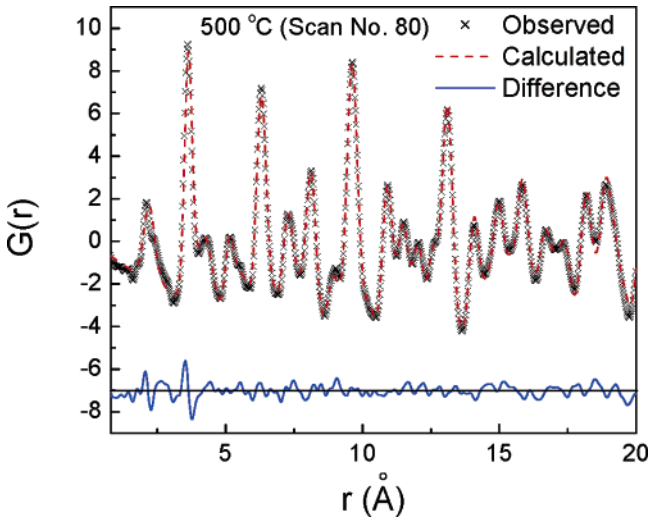

Figure 12. Real space Rietveld analysis of $G(r)$ for scan no. 80.

Zr L_{II} and L_{III} spectra for monoclinic ZrO_2, cubic YSZ, and amorphous zirconia are shown in Figure 14. Similar to the cubic (Zr, Ce, Sm)O_{2-x}, cubic YSZ shows two white main peaks, A (e_g) and B (t_{2g}), in both spectra. The monoclinic ZrO_2 shows a small C peak between A and B, which can also be explained by decreased crystal symmetry similar to that of tetragonal zirconia. The line shape of amorphous phase is similar to that of cubic ZrO_2, but different from those of tetragonal and monoclinic zirconia. Figure 15 shows the peak-fit of the Zr L_{III} edge XANES spectra of amorphous zirconia. An arctangent function is used to simulate the edge jump, whereas the arctangent function together with two Gaussian peaks provide satisfactory fitting to the original spectrum from amorphous ZrO_2. More importantly, the two peaks are separated by 2.3 eV, which is same as the A−B separation in the cubic phase.

4. Discussion

The phase-stabilization mechanism of ZrO_2 is complicated. It has been found that when ZrO_2 is reduced to ZrO_{2-x}, the cubic phase can be stabilized at room temperature.[39] A recent

(39) Chatterjee, A.; Pradhan, S. K.; Datta, A.; Datta, M.; De, M.; Chakravorty, D. *J. Mater. Res.* **1994**, *9* (2), 263.

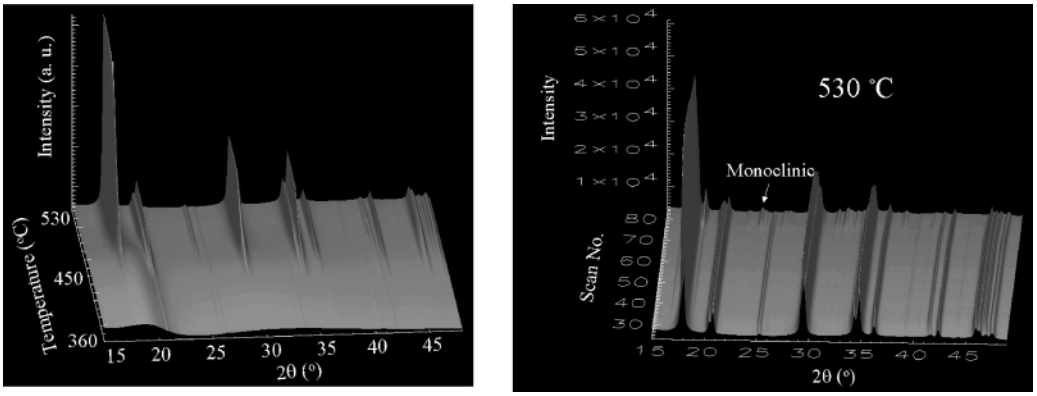

Figure 13. In situ high-temperature XRD of amorphous ZrO_2 in an oxidizing environment (P_{O_2} = 38 torrs) (a) Ramping from room temperature to 530 °C. See the emergence of the tetragonal phase around 450 °C. (b) Dwelling at 530 °C. See the emergence of the monoclinic phase at scan no. 80.

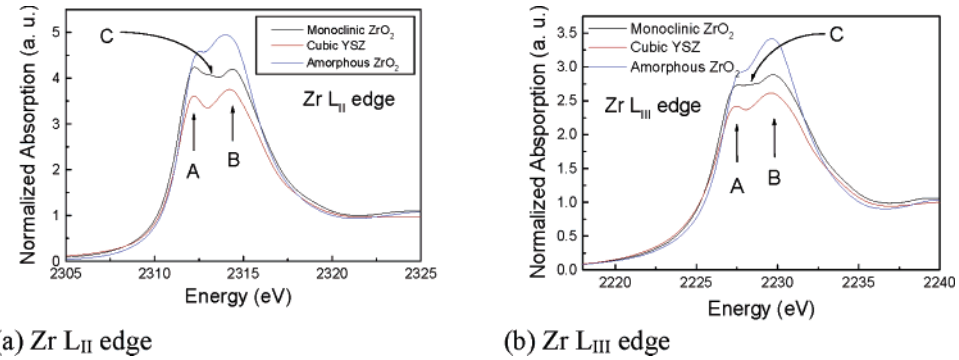

Figure 14. Zr L_{II} and L_{III} spectra of the monoclinic ZrO_2, the cubic yttria-stabilized zirconia (YSZ), and the amorphous ZrO_2.

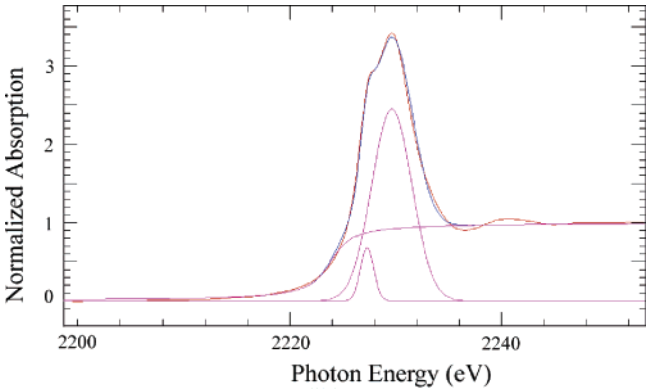

Figure 15. Peak-fitting of the Zr L_{III} edge spectrum of amorphous ZrO_2.

density function theory calculation on pure ZrO_2 shows that 4% oxygen vacancy alone is enough to stabilize the cubic phase at room temperature.[8] With the results presented in this study, the crystallization from amorphous to crystalline zirconia is affected by the gaseous environment during annealing. From the real space Rietveld PDF analyses, the oxygen occupancy is about 97%, indicting 3% oxygen vacancies. A different Rietveld analysis with Zr occupancy of 97% gives a higher concentration of oxygen vacancies of 16%. Although the 3% oxygen vacancy concentration value agrees well with the theoretical calculation,[8] a direct calculation from the Zr−O coordination number of 7.3 gives an oxygen vacancy concentration of 8.7%, which lies between the two values from Rietveld analysis, indicating that the results are reasonable.

It is widely accepted that the structure of the amorphous ZrO_2 is closer to tetragonal phase,[40,41] although Winterer demonstrated it to be closer to cubic phase.[15] When the Zr−O and Zr−Zr coordination numbers of amorphous phase are compared with those of the other zirconia polymorphs obtained from this study and previous EXAFS studies,[12−13] the structure of the amorphous phase is concluded to be closer to the cubic phase. The XANES result also proves that the local structure of amorphous zirconia is similar to that of cubic phase, which can be a direct result from the present preparation method of nanoparticles of amorphous ZrO_2.

Here, the results show good agreement with the previous EXAFS results, indicating that this PDF analysis, which is based on in situ synchrotron XRD technique, is promising. With future instrumental improvements, e.g., newer generation synchrotron X-ray sources and better area detectors, the quality of the XRD pattern and the acquisition time will be improved, making this technique more powerful.

Conclusions

The synchrotron X-ray with high intensity coupled with an image plate detector enables in situ XRD study extended to high Q values, allowing the present structural analysis of the phase transition from amorphous to cubic zirconia. The local structure of the amorphous zirconia closely resembled that of cubic ZrO_2, but not tetragonal zirconia, which is corroborated by the results of X-ray absorption near edge spectroscopy (XANES) at Zr L_{II} and L_{III}. Under a reducing

(40) Molodetsky, I.; Navrotsky, A.; Paskowits, M. J.; Leppert, V. J.; Risbud, S. H. *J. Non-Cryst. Solids* **2000**, *263* (1−3), 106.
(41) Livage, J.; Doi, K.; Mazieres, C. *J. Am. Ceram. Soc.* **1968**, *51* (6), 349.

condition of $P_{O_2} = 1 \times 10^{-7}$ Torr, the amorphous phase directly crystallizes to cubic ZrO_{2-x} at 434 °C. Oxygen vacancies may play an important role in stabilizing the cubic phase. In $P_{O_2} = 38$ Torr, the amorphous ZrO_{2-x} directly crystallizes to the tetragonal phase, even when the particle size is ~3 nm. The crystallization of amorphous zirconia is drastically affected by the gaseous environment, particle size, and oxygen vacancy concentration.

Acknowledgment. S.L.A.L. acknowledges the Hong Kong Bank Foundation Overseas Scholarship for the financial support. The Advanced Photon Source is supported by the U.S. Department of Energy, Office of Science, Office of Basic Energy Sciences, under Contract W-31-109-Eng-38. Research carried out at the NSLS, BNL, is supported by the U.S. Department of Energy, Division of Materials Sciences and Division of Chemical Sciences, under Contract DE-AC02-98CH10886. This work is supported by the MRSEC Program of the National Science Foundation (DMR-0213574), the New York State Office of Science, Technology and Academic Research (NYSTAR) and the Department of Energy under BES/HFI Grant DE-FG02-05ER15730.

CM061739W